Atmos. Chem. Phys. Discuss., https://doi.org/10.5194/acp-2018-1307
Manuscript under review for journal Atmos. Chem. Phys.
Discussion started: 23 January 2019

Atmospheric Chemistry and Physics Discussions

Specifying light absorbing properties of aerosol particles in fresh snow samples, collected at the Environmental Research Station Schneefernerhaus (UFS), Zugspitze

Claudia Linke[1], Inas Ibrahim[1], Alexei Kiselev[1], Fritz Waitz[1], Thomas Leisner[1], Till Rehm[2], Stefan Norra[3] and Martin Schnaiter[1,4]

[1]Institute of Meteorology and Climate Research, Atmospheric Aerosol Research, KIT, Karlsruhe, Germany
[2]Environmental Research Station Schneefernerhaus (UFS), Zugspitze, Germany
[3]Institute of Geography and Geoecology, IfGG, Karlsruhe, Germany
[4]schnaiTEC GmbH, Zell a. H., Germany

Correspondence to: Claudia Linke (Claudia.Linke@kit.edu)

Abstract

Darkening of pristine white areas on Earth could happen when light absorbing particles are deposited on snow and ice surfaces. Airborne particles like mineral dust, ashes or carbonaceous aerosols are able to reduce the snow and ice albedo already by a small quantity of deposited particles. In this study we developed a laboratory analysis method to address mass and absorption properties of snow particles simultaneously. For a set of snow samples, taken at the Environmental Research Station Schneefernerhaus (UFS) during winter 2016/2017, we combine the determination of refractory Black Carbon mass (rBC) by a Single Particle Soot Photometer (SP2) with photo acoustic aerosol absorption spectroscopy at three distinct wavelengths across the visible spectral range (PAAS-3λ). For the calibration of the method, "Fullerene" standard aerosol was used and its mass specific absorption cross section was determined. The analysis of the UFS snow sample measurements reveals a significant difference between the particle masses determined from the PAAS-3λ and the SP2 data. Our findings suggest that the light absorbing particles included in the snow could not only be composed of rBC but must have particulate matter of different nature. This result is confirmed by Environmental Scanning Electron Microscopy (ESEM) and single particle fluorescence measurements with the Waveband Integrated Bioaerosol Sensor (WIBS-4) which both revealed a significant portion of biological material to be present in the snow samples.

1. Introduction

Naturally released aerosols like mineral dust or volcanic ash as well as anthropogenic carbonaceous aerosols like black carbon (BC) are airborne particles which finally are deposited on the ground. Light absorbing particles settled on snow or ice surfaces can significantly reduce the snow or ice albedo. The otherwise white surface becomes darker resulting in an increased absorption of solar radiation in the snow and ice packs (Doherty et al., 2010; Ramanathan and Carmichael, 2008). Because pure snow is the most reflective natural surface on earth, the presence of small amounts of absorptive impurities, such as BC and dust particles in snow, reduce the albedo considerably (Warren, 1982). This reduction then contributes to the so-called snow-albedo feedback, the metamorphosis and eventually the retreat of snow covers in a warming climate. The IPCC 2013 reported a global annual mean radiative forcing for anthropogenic BC in snow and ice of + 0.04 W m^{-2} with an uncertainty range of 0.02 to 0.09 Wm^{-2} (5th and 95th percentiles). A considerably higher estimate from BC deposition in snow and

sea ice was given by Bond et al. (2013). They combined forcing results from radiative transfer, rapid adjustment and snow albedo feedback resulting in a best forcing estimate of + 0.13 W m^{-2} with an uncertainty of 0.04 to 0.33 W m^{-2} (90% uncertainty bounds). In cold fine-grained snow the BC amounts can reduce the spectral albedo at visible wavelengths by 0-2%, in melting snow these reductions can even increase to 1-6%, representing a significant climatic forcing (Clarke and Noone, 1985; Warren, 2013).

Not only Arctic (Clarke and Noone, 1985) and Antarctic (Bisiaux et al., 2012) regions but also glaciers and permafrost regions in the mountains (Jacobi et al., 2015; Kaspari et al., 2014; Li et al., 2016; Painter et al., 2007; Schmitt et al., 2015) are affected. In Arctic snow and ice the light absorbing aerosols are considered to be the important factors leading to a rapid melting (Bond et al., 2013; Clarke and Noone, 1985; Warren, 1982). The snow-albedo feedback is accelerating over springtime Eurasia, which had lost about 14% of its snow cover since 1979 and warmed more rapidly during the last 30 years (0.64°C per decade) than most other locations and seasons on earth (Flanner et al., 2009; Flanner et al., 2007). Doherty et al. (2010) and Flanner et al. (2007) resumed measurements of BC from Greenland and the Arctic and reported for BC in snow values between 2 ng g^{-1} and 60 ng g^{-1}.

Soot is the most efficient absorbing constituent of the atmospheric aerosol and 1 ng g^{-1} of soot in snow has approximately the same effect on the albedo as 100 ng g^{-1} of dust in the visible wavelength range at 500 nm (Warren, 1982). Even if dust is a less efficient absorber than soot the dust mass loads detected in the Greenland ice shield might be able to achieve values to an extend of 500 ng g^{-1} (Dumont et al., 2014) thus significantly contributing to the albedo reduction. To assess the impact of impurities in snow the authors performed a numerical experiment and reduced the broadband albedo of snow in their model by 0.01 thus simulating the increase of snow impurity content. Their results show enhanced sublimation everywhere and enhanced snow melt at low elevations. Doherty et al. (2010) showed that 20–50% of the light absorption by particles in the arctic snowpack is by non-black carbon constituents, such as brown carbon and dust (Doherty et al., 2010). The springtime melt period in Sodankylä, Finland was observed during the Snow Reflectance Transition Experiment (SNORTEX) in April 2009 (Meinander et al., 2013). The authors determined albedo values of only 0.5 – 0.7 for the ultraviolet and visible wavelength range. The ultraviolet and visible albedo for clean snow should be about 0.97-0.99. They explain the low albedo values amongst other reasons with the absorption of BC and OC impurities in the snow of 87 ppb and 2894 ppb, respectively.

Most Himalayan glaciers as glaciers elsewhere have retreated and lost mass since the mid-19th century .When dust concentrations are high, dust dominates absorption, snow albedo reduction and radiative forcing and the impact of BC may be negligible (Bolch et al., 2012; Kaspari et al., 2014). Zhang et al. (2018) estimated the effects of BC and dust on glaciers and snowmelt across the Tibetan Plateau based on the simulations of albedo reduction and radiative forcing. They found that glacial snowmelt water caused by light absorbing particles contribute to about 20% of the glacier mass loss (Zhang et al., 2018).

Despite their significance for the snow albedo feedback, the light absorbing particles in snow are poorly investigated regarding their chemical, microphysical, and spectral optical properties. In the last decades particularly mass concentrations of light absorbing particles in snow were determined. For comparison purposes, BC mass concentrations were recalculated from optical methods by accepted mass specific absorption cross sections (MAC). Therefore filter based spectrophotometry measurement techniques (Clarke and Noone, 1985;

Doherty et al., 2010; Grenfell et al., 2011; Wang et al., 2013; Zhou et al., 2017) or filter based thermo-optical analysis (Forsström et al., 2009; Lim et al., 2014)) were used to gain BC mass concentrations from snow samples.

Based on the method given in Clarke and Noone (1985), Grenfell et al. (2011) developed an Integrating Plate-Integrating SandWich (ISSW) spectrophotometer where the melted snow samples are deposited by filtration on filters for optical analysis. The ISSW determines the total absorption of the particles in the snow sample in range of visible and near-UV solar radiation and is able to discriminate between the fraction of BC and non-BC. Under the assumption that all absorption in the wavelength range between 650 nm and 700 nm is due to BC, an upper BC mass concentration is determined by the use of an absorption Angström exponent of one. The BC mass concentrations are then quantified using MAC values of the Monarch-71 soot standard.

For the thermo-optical analysis of snow or ice samples in terms of their EC and OC mass content, the melted samples are filtrated on Quartz filters, which are subsequently heat treated with a defined temperature protocol. Following this protocol, the filter is first heated under inert conditions to desorb OC. After cooling of the filter it is reheated in several temperature steps under a Helium/Oxygen atmosphere where EC is oxidized under defined conditions (Forsström et al., 2009; Lim et al., 2014). Forsström et al. (2009) used an EC/OC Sunset instrument with NIOSH 5040 temperature protocol to analyze snow samples

A further method without filtration is now given with the Single Particle Soot Photometer (SP2) combined with a nebulizer to aerosolize the particles after melting of the snow sample (Katich et al., 2017; Lim et al., 2014; Schwarz et al., 2012). The single particle soot photometer (SP2) analyses spectral thermal radiation of laser-heated particles. The calibration of the instrument with “Fullerene” soot delivers a refractory Black Carbon (rBC) mass concentration. The combination of SP2 with a nebulizing system like APEX-Q (Lim et al., 2014) or CETAC (Bisiaux et al., 2012; Katich et al., 2017) offers the possibility to aerosolize a melted snow sample to measure the rBC mass concentration.

Overall, the measurement methods to deduce the BC mass concentration in snow and ice samples were advanced and improved over the past decade. However, the above methods and studies are solely focused on the mass concentration of the particles in the samples but give no information of their light absorption properties. In order to quantify the influence of deposited aerosol particles on the solar albedo of snow and ice fields, it is conclusive that it is at least equally important to quantify the particle light absorption properties in conjunction with the particle mass concentration (Grenfell et al., 2011). Currently, there is a lack of knowledge regarding the nature of the light absorbing particles in snow as more or less all of the above methods determine the mass concentration of refractory BC. This is certainly justified by the fact that BC is the strongest absorbing component of the atmospheric aerosol, but does not answer the question what is the contribution of other light absorbing materials like mineral dust or OC on the overall solar albedo of snow and ice surfaces.

In this study we present for the first time the simultaneous measurements of the refractory BC mass concentration and the visible light absorption coefficient of the re-aerosolized particles from snow samples. Using a typical refractory BC material, which in our case is “Fullerene” soot, we are able to determine the mass specific absorption cross section (MAC) for this material by concurrent photo acoustic absorption and SP2 mass measurements. With this MAC we are able to recalculate a “Fullerene” soot equivalent mass concentration from our photo acoustic measurements of snow samples at three wavelengths and can directly compare this optically

active mass with the BC mass concentration from the SP2 measurement. Sample preparation, test particle properties and experimental setup are given in Sect. 2. Sect. 3 describes the characterization of the used nebulizer at different operational settings and gives the efficiency of the nebulizer in terms of particle number and mass concentrations. The deduced three wavelengths MAC of "Fullerene" soot is presented in Sect. 4. The measurement results of our snow samples are discussed Sect. 5 followed by conclusions given in Sect. 6.

2. Experimental

2.1 Snow samples

The snow samples used in this study originate from the Environmental Research Station Schneefernerhaus (UFS). The station is located at a latitude of 47° 25' 00'' N, a longitude of 10° 58' 46'' E and an altitude of 2650 m a.s.l. During winter the UFS is situated in the free troposphere most of the time with low boundary layer influence but can be occasionally affected by long range transported Saharan dust plumes (Flentje et al., 2015; Israelevich et al., 2012). However, the station is located within a skiing and hiking resort and, therefore, might be regularly affected by local anthropogenic emissions, e.g. from snow groomers during the skiing season. The samples were collected during a time period from December 2016 to May 2017. During this time period basic meteorological data of precipitation, maximum and minimum temperatures, sunshine duration and wind speed are provided by the German Meteorological Service (DWD). Aerosol parameters like number concentrations from condensation particle counter (CPC) and optical particle counter (OPC) instruments, BC mass concentrations from multi-angle absorption photometer (MAAP) measurements as well as dust loads are provided from the German Environment Agency (UBA) and the German Meteorological Service (DWD). Each time after snowfall a sample of fresh snow was collected outside the UFS from the approximately 10 cm deep top layer of a predefined 60 x 40 cm sampling area located at platform 7 of the station at 2678m a.s.l using a metallic hand shovel. During the winter season this place is highly exposed to wind and sunshine (Risius et al., 2015). After collection, the samples were sealed in polyethylene household plastic bags with zipper seal (1 liter volume, Toppits, Germany) and were stored at the UFS in a freezer at -18°C until they were transported under frozen conditions to the laboratory. During six months 33 samples were taken at the UFS.

The determination of the light absorbing properties of the snow samples implies that the insoluble light absorbing particles have to be isolated from the enclosing snow matrix. To get rid of the snow the samples were melted right before the measurement in an ultrasonic bath (EMAG Technologies, Germany) at room temperature for 5 minutes. The melted snow samples were then analysed as described in the following.

2.2 Setup of instruments

The experimental setup consisting of a Marin-5 Enhanced Nebulizer System (Teledyne CETAC Technologies, USA), a self-built three-wavelength photo acoustic aerosol absorption spectrometer (PAAS-3λ, Linke et al., 2016) and a single particle soot photometer (SP2, DMT, USA) is shown in Figure 1. The liquid samples were fed by a peristaltic pump (Ismatec, ISM 795C, Germany) equipped with Tygon tubing (ID 0.76mm, E-LFL) into a concentric pneumatic glass nebulizer (Micromist 500), which is positioned inside of the Marin-5 nebulizer. The glass nebulizer consists of a capillary for the liquid sample at whose tip a concentrically sheath flow of pressurized synthetic air ends up dispersing the liquid phase into a spray (Katich et al. 2017). For most effective

dispersion the glass nebulizer is mounted with an angle in the spray chamber. With a maximum flow rate of 500 µL per minute the glass nozzle aerosolizes the liquid into a droplet spray, which is released into the nebulizing chamber of the Marin-5 nebulizer, see Figure 2. The spray enters the heated part of the chamber where the water is evaporated forming a moist aerosol of residual particles. This aerosol comprises refractory and soluble aerosol particles that were deposited in the snow sample. Subsequently, the aerosol passes the cooled part of the chamber where excess water is eliminated from the sample flow by condensation so that the bulk of water is removed before the particles leave the nebulizer. The aerosol that left the nebulizer is then directed through a dryer (Figure 1) to reduce the relative humidity of the sample flow below 20% r.h. Finally, the sample flow is split and one part is led through the SP2 while the other part is directed into the PAAS-3λ.

The SP2 was used to determine the refractory black carbon (rBC) mass concentration of calibration standards and the snow samples. With a flow rate of 0.12 L min^{-1} the sample enters the instrument. For mass detection the incandescence signal of the instrument was calibrated with “Fullerene” soot particles (Alfa Aesar, Lot F12S011) size selected by a differential mobility analyser (DMA) in the range of 100 nm to 450 nm, corresponding to rBC masses of about 0.5 fg to 30 fg. In addition, to quantify the efficiency of the nebulizer, number concentrations of non-absorbing PSL particles were determined from the SP2 scattering signal. For analysis of the SP2 data the software toolkit developed and provided by Martin Gysel from Paul Scherrer Institute, Switzerland was used (Gysel et al. 2011).

The PAAS-3λ is a single cavity three-wavelength photoacoustic aerosol absorption spectrometer, which has been designed and built at KIT and which is currently marketed by schnaiTEC GmbH. The instrument concept and working principle are described in detail in Linke et al. (2016). Briefly, to measure the absorption coefficient of aerosols, a controlled sample flow of 0.85 L min^{-1} is led through the acoustic cavity of the instrument. This open-ended acoustic resonator has a diameter of 6.5 mm and a length of 49 mm resulting in a fundamental resonance frequency of about 3200 Hz. Acoustic buffers of 24.5 mm length and 78 mm diameter are attached to both ends of the resonator tube to filter acoustic disturbances that may exist in the frequency range of the resonator. Possible disturbances comprise noise generated in the flow system as well as ambient sound. The system was developed to determine the absorption coefficients at three wavelengths across the visible spectral range. Three modulated lasers are used in this study emitting at 405 nm, 532 nm and 658 nm (Dragonlaser, China) and with modulated emission power of 100 mW,150 mW, 130 mW, respectively. The modulation frequency is regularly tuned to the resonance frequency of the acoustic cavity by ramping frequency scans. The detection limit (2σ) of this setup was derived from an Allan deviation analysis of long-term background signal measurements similar to the analysis presented in Fischer and Smith (2018) (Fischer and Smith, 2018). The Allan deviation plot for the three PAAS-3λ wavelengths is shown in Figure 3. According to this analysis the PAAS-3λ instrument has a 2σ detection limit of about 1.4 10^{-6} m^{-1} for all three wavelengths at an averaging time of 60 seconds.

2.3 PSL particles

The characterisation of the particle number efficiency of the nebulizer and the daily performance control was performed with monodisperse polystyrene latex spheres (PSL) particles (Postnova, Thermo Scientific) with nominal diameters of 240±5 nm and 304±5 nm. The particle number concentration within these suspensions was

about 3 10^8 mL^{-1} (Thermo Scientific). A diluted PSL standard suspension sample was prepared daily by pipetting 1 ml suspension into a 100 ml graduated flask filled with nanopure water.

2.4 "Fullerene" Soot Standards

Suspensions of known "Fullerene" soot concentration were prepared to determine the particle mass efficiency of the nebulizer. For that a "Fullerene" soot stock suspension of nanopure water was prepared from "Fullerene" soot particles (Alfa Aesar, Lot F12S011) and allowed to settle large particles for several days (Schwarz et al. 2010). From this stock suspension the supernatant suspension was taken (a) to determine the "Fullerene" soot mass concentration gravimetrically and (b) to prepare diluted "Fullerene" soot standard suspensions in nanopure water for daily particle mass efficiency control of the nebulizer.

For the gravimetric analysis of the settled stock suspension two empty quartz fiber filters (Munktell MK360) were dried over night at 50°C, stored in a dehydrator for 2 hours and weighted with a microbalance (Sartorius micro M3P). Then 30 ml of the supernatant suspension were extracted from the stock "Fullerene" soot suspension and were dropped on both quartz filters. The filters were then temperature treated the same way as the empty filters before and were finally weighted. From the determined gravitational "Fullerene" soot mass, the mass concentration of the stock suspension was determined to be 5.8 ± 2.6 µg g^{-1} (N=2). Four "Fullerene" soot standard suspensions for daily characterizations of the mass efficiency of the nebulizer were daily prepared from the stock suspension in two dilution steps with nanopure water resulting in "Fullerene" soot suspensions with mass concentrations c_{FS} of 11.5, 23, 34.5 and 46 ng mL^{-1}. These "Fullerene"soot standard suspensions were used to determine the fraction of "Fullerene" soot particle mass that is aerosolized by the nebulizer.

3. Characterization of the nebulizer

The particles within a liquid sample are not completely dispersed during the nebulizing process in the Marin-5 nebulizer. Depending on the settings a smaller or larger fraction of particles or particle mass is aerosolized into the sample flow while the rest is lost and drained off with the excess water (Katich et al., 2017).

According to Katich et al. (2017), for optimal operation conditions of the Marin-5 nebulizer, we adapted their recommendations to our necessities. To determine the absorption coefficients of the particles deposited in the snow samples it is necessary to fill the complete volume of the photo acoustic cell with the aerosol generated from the snow samples. This requires a sample volume flow rate that is significantly larger than that required for the SP2 based rBC measurement alone. Also, the relative humidity of the sample is important for a reliable absorption measurement with the PAAS-3λ (Langridge et al., 2013). Both the dispersion efficiency (in terms of particle number and mass) and the relative humidity are depending on the flow rates of the liquid sample and the synthetic air flow. This is also valid for the temperature of the heating chamber of the Marin5. As a starting point the nebulizer parameter were set to heating and cooling temperatures of 120°C and 5°C, respectively, a synthetic air flow of 1.1 L min^{-1} and a supply liquid sample flow of 0.08 mL min^{-1}. Each parameter was varied while keeping the others constant. It turned out that the temperature of the cooling chamber has only a minor influence on the dispersion efficiency and the relative humidity in the exit flow.

Atmos. Chem. Phys. Discuss., https://doi.org/10.5194/acp-2018-1307
Manuscript under review for journal Atmos. Chem. Phys.
Discussion started: 23 January 2019

In Figure 4, the dependencies of the PSL particle number concentrations and the relative humidity of the Marin-5 exit flow are displayed for increasing gas flow rates of the nebulizer. The synthetic air flow was adjusted with a mass flow controller (MFC) within the operation limits of Marin-5 nebulizer between 0.6 L min^{-1} and 1.1 L min^{-1}. The higher the input flow of synthetic air the higher the PSL number concentrations and the relative humidity at the exit. In a uniform manner the PSL number concentrations and relative humidity continuously increase with increasing liquid flow (not shown). Regarding the influence of the temperature applied to the heated section of the nebulizer chamber, both the PSL particle concentrations and the relative humidity increase with increasing temperature (not shown).

While the SP2 only needs a low sample flow rate of 0.12 L min^{-1}, the sample flow rate required for the simultaneous photo acoustic measurements is significantly larger, because of the relatively large volume of the photo acoustic cell of 236 cm^3 including the buffer volumes. As a consequence of this it was necessary to run the Marin-5 nebulizer with its maximum gas flow output of 1.1 L min^{-1} synthetic air. To ensure sufficient cell volume exchange the cell was flushed at least five times before each sample and each background measurement. The sample flow rate was controlled daily behind the drier with a gas flow meter (Gilibrator, Sensidyne). This measurement assured a SP2 volume flow rate of 0.12 L min^{-1} and a PAAS-3λ volume flow rate of 0.85 L/min while the excess volume gas flow of 0.13 L min^{-1} was directed through a filter to the ambient. The supply liquid sample flow of the Marin-5 nebulizer was then fixed at a rate 0.32 mL min^{-1}, which guarantees a high enough particle mass concentration for the photo acoustic measurement. The heating and cooling temperatures were set to 120°C and 5°C, respectively. The relative humidity for the aerosolized snow samples under these operation conditions always ranged between 10% and 20% downstream the drier, which is low enough for photoacoustic absorption measurements that are not influenced by humidity (Langridge et al., 2013).

With the above settings, the nebulizing efficiency $\varepsilon = (c_{SP2}/c_{FS})*(R_{gas}/R_{Liquid})$ of the Marin-5 nebulizer was derived from "Fullerene" soot standard suspensions with given concentrations of c_{FS}. The rBC mass concentration c_{SP2} measured by the SP2 in conjunction with the set liquid and gas flow rates R_{liquid} and R_{gas}, respectively, then define the fraction of "Fullerene" soot mass that makes it from the suspension into the aerosol flow. In Figure 5 the detected SP2 mass concentrations are shown for the four "Fullerene" standards which were daily prepared. The nebulizing efficiency was determined to be 36% from these measurements, which is in good agreement with the findings of Katich et al. (2017) for the same settings.

4. Specific mass absorption cross sections of "Fullerene" soot

Simultaneously to the rBC mass concentration measurements with the SP2, the absorption coefficients of the "Fullerene" soot standards were measured for the three PAAS-3λ wavelengths. Both measurements together enable the determination of the mass specific absorption cross section (MAC) of "Fullerene" soot at 405, 532, and 658 nm. In Figure 6, the absorption coefficients are plotted against the SP2 derived rBC mass concentrations of the "Fullerene" soot standards. Linear regression fits of the data result in MAC values of 11.8 ± 3.8 m^2g^{-1} for 405 nm, 10.6 ± 2.8 $m^2 g^{-1}$ for 532 nm and 9.7 ± 3.9 $m^2 g^{-1}$ for 658nm. The 532 nm MAC is significantly higher than the respective value published in Zhou et al. (2017), who reported a MAC_{real} value for "Fullerene" soot measured with ISSW at 550 nm of 6.4 ± 0.4 $m^2 g^{-1}$. Generally, as the MAC of rBC particles are dependent on the actual size of the particles (especially in the sub-500 nm range), differences in reported MAC values of the same

particulate material may be caused by differences in the actual size distributions used in the different studies (Garcia-Fernandez et al., 2015).

The wavelength dependence of the aerosol light absorption, expressed by the so-called absorption Angström exponent AAE, was determined to be 0.48 ± 0.09 for the used "Fullerene" soot standard. The Angström Exponent found for "Fullerene" soot here compares quite well with results for "Fullerene" soot from a workshop addressed to soot reference materials (Baumgardner et al., 2012), where an an Angström exponent for "Fullerene" soot of about 0.6 was reported from multiwavelength PSAP and Aethalometer measurements, and to Zhou et al. (2017) who determined an absorption Angström Exponent between 450 nm and 750 nm of 0.54 ± 0.06.

5. Results of the snow sample measurements

The instrumental setup was used to measure a set of 33 snow samples from the UFS in the same way as the "Fullerene" soot standards before. The measured rBC mass concentration of the aerosolized snow samples shown in Figure 7 was corrected for the Marin-5 nebulizing efficiency to determine the rBC_{SP2} mass concentration of the snow samples. Figure 8 shows the associated mass size distribution of the measured particles averaged over all snow samples shown in Figure 7. The SP2 rBC mass measurements only include particles up to a mass equivalent diameter of 500 nm, which means that larger rBC particles would not be recorded by the SP2. However, the rBC mass size distribution peaks around 190 nm with a clear decrease to larger sizes. Thus, the majority of the rBC particles in fresh snow samples have sizes below 0.6 µm, which implies that the snow hasn't experienced thaw/freezing cycles (Schwarz et al., 2013).

A "Fullerene" soot absorption equivalent rBC mass concentration of the snow samples was determined from the PAAS-3λ absorption coefficients by applying the MAC values determined for "Fullerene" soot at the three wavelengths. This absorption derived mass concentration is henceforth referred to as PAAS-3λ equivalent rBC mass concentration rBC_{PAAS}. In Figure 9, rBC_{PAAS} mass concentrations of the snow samples are plotted against the corresponding rBC_{SP2} concentrations. The black dashed line represents the 1:1 line that would be expected if "Fullerene" soot was the only absorbing aerosol mass in the snow. From this figure it is obvious that the observed light absorption of the aerosol particles in the snow samples could not completely be traced back to rBC_{SP2} aerosol mass, i.e. aerosol mass that has a high enough absorption cross section in the near-infrared spectral region to generate an incandescence signal in the SP2. Interestingly, the enhancement factors of the rBC_{PAAS} concentrations with respect to rBC_{SP2} concentrations are not constant but increase with decreasing wavelengths with values of 1.65, 2.28, and 2.38 for 658, 532, and 405 nm, respectively. This observation suggests that part of the absorbing aerosol mass in these samples might be mineral dust or brown carbon (BrC) that is co-deposited with the rBC_{SP2} mass (Hoffer et al., 2006; Kirchstetter and Thatcher, 2012; Linke et al., 2016; Linke et al., 2006; Müller et al., 2011). It is conclusive that these kinds of aerosol mass are present in the ambient air at the UFS. In addition, the mean AAE of the snow samples for the spectral range between 405 nm and 658 nm has a value of 1.25 ± 0.86 which is significantly larger and more varying than 0.48 ± 0.09 deduced for the "Fullerene" soot standard in the same spectral range. This also indicates the presence of other optically more variable material in the snow that predominantly absorb in the blue part of the visible spectrum.

During the period of time when the snow samples were taken at the UFS no correlation was found between our snow sample analysis results and the concurrent meteorological data of precipitation amount, wind speed, temperature, sunshine duration and snow height. Not even a correlation was found between our snow sample data and ambient air BC mass concentrations that are continuously monitored at the UFS Station. On the other hand, Saharan dust events that are detected by the DWD from ceilometer measurements and that are given as a daily Saharan dust index (SDI) show that, within each month between December 2016 and May 2017, the atmosphere in southern Germany was influenced for several days by Saharan dust. (https://www.dwd.de/EN/research/observing_atmosphere/composition_atmosphere/aerosol/cont_nav/sahara_dust_index.html)

To get a general idea of the nature of the components that are solved and dissolved within the snow samples ionic chromatography (IC) and an inductive coupled plasma mass spectrometry (ICP-MS) analysis were exemplarily conducted for the snow sample from March 10, 2017, mainly to clarify the concentration of higher ions which might be present in the snow. Additionally, the aerosol released from this snow sample was fed to a Waveband Integrated Bioaerosol Sensor (WIBS4) to get information on the biological particle fraction. A Nuclepore filter was taken for ESEM microscopy to further characterize the different particle types found mainly in the larger particle size range (larger than ~500 nm) of this sample. The sampling for WIBS4 instrument and for the Nuclepore filter was performed behind the dryer downstream the nebulizing system by substituting the PAAS-3λ and the SP2 (see Figure 1).

The snow sample from March 10, 2017 has a mass concentration of rBC_{SP2}=2.3 ng/ml and an absorption equivalent mass concentration of rBC_{PAAS}=6.3 ng/ml for λ=405 nm, which gives a mass enhancement factor of 2.7. The sample is therefore representative for all samples. The IC analysis of the snow sample conducted for anionic ions shows only little concentrations of chloride, nitrate and sulphate of 0.29, 1.1 and 0.3 mg L^{-1}, respectively. Only very low concentrations of alkaline and alkaline earth metals were found from the ICP-MS analysis. For the trace metals manganese, iron, copper and zinc concentrations of 9.7 µg L^{-1}, 1.7 µg L^{-1}, 1.1µg L^{-1} and 8.7µg L^{-1} were found, respectively.

The ESEM micrographs (ThermoFischer Scientific) combined with EDX microanalysis (EDAX, Octane Elite Super) reveal that the larger (>~500 nm) particles extracted from the snow sample predominantly consist of biological materials, such as fragments of cellular membrane, whole bacteria, pollen, spores, and their mixtures. The mineral dust particles could be identified in the sample too, but to a much less extent than the biological particles. Figure 10 gives an overview composite image of a typical Nuclepore® filter area, where particles with heavier elements like Al, Si, Fe, Mg, K, and Ti, are accentuated in green colour due to their brighter response in backscatter electron detector (BSED). These elements are typically found in mineral dust particles, as compared to the lighter elements like C, N, O, Na, and S, typical for biological material. This overview picture highlights the low relative abundance of the mineral dust particles in the coarse mode particle size range of the sample. Representative examples of individual particles are given in the figures 11 to 13. Note that EDX spectra of all individual particles are very characteristic for particle agglomerates or for chemical aging: thus, the biogenic particle (Figure 11) has areas showing intracellular composition (spot A) and pure cellular membrane fragment (spot B), whereas the mineral dust particle (Figure 12) and soot particle (Figure 13) exhibit spectra characteristic both for inorganic and biogenic material. The particle of “Fullerene” soot, produced from aqueous suspension

exactly in the same way as the other residual particles discussed above, is shown in Figure 14. As expected, the "Fullerene" soot particle does not contain any foreign chemical elements, as shown by the EDX spectrum in the right panel of Figure 14.

The WIBS4 detects biological aerosol particles by combining single particle fluorescence signals in two wavebands (FBAP). The WIBS4 measurement of the March 10, 2017 snow sample supports the ESEM results of a high fraction of biological particles (43%) in the size range larger than 0.5 µm. The size segregated analysis reveals biological particle fractions of 80% and 100% for sizes larger than 2 µm and 3 µm, respectively.

One question that arises from the above findings is whether the biogenic particles found in our snow samples can be related brown carbon (BrC). The term brown carbon is not clearly defined or characterized. It is expected that brown carbon are particles released during incomplete combustion processes (Wu et al., 2016). BrC is also found in fresh and photochemically aged biomass burning emissions (Saleh et al., 2013). In other studies, BrC was chemically divided into humic-like substances (HULIS) and tar balls (Chakrabarty et al., 2010; Wu et al., 2016). While HULIS can be characterised mainly as a mixture of macromolecular organic compounds with various functional groups, tar balls are emitted from biomass burning and are of spherical, amorphous structure and are typically not aggregated. Moreover, light absorbing organic material and humic-like substances can be present in the water-soluble fraction of ambient particulate matter (Moschos et al., 2018; Phillips et al., 2017). Further examination of snow samples from different locations as well as systematic investigations on the optical behaviour of biological particulate matter is therefore necessary to evaluate the influence of biological and biogenic particulate matter on the aerosol absorption properties in the visible spectral range.

6. Conclusions

In this study we present a novel laboratory analysis method for snow and ice samples that allows for the first time (a) the direct photoacoustic (PAAS-3λ) measurement of the aerosol absorption coefficients of re-aerosolized snow samples over the visible spectral range, i.e. without depositing the particles on filters, and (b) the concurrent measurement of the refractory black carbon (rBC_{SP2}) mass concentration of the snow particles using a single particle soot photometer (SP2). Using water suspensions of "Fullerene" soot particles of known rBC_{SP2} mass concentrations as a reference for the snow samples, (a) the rBC_{SP2} mass specific absorption cross section (MAC) of the suspended "Fullerene" soot particles could be determined for three wavelengths in the visible at 405, 532 and 658 nm and (b) the mass aerosolization efficiency of the nebulizer could be quantified. The MAC values were then applied in the analysis of 33 snow samples, which were collected at the Environmental Research Station Schneefernerhaus (UFS) in the winter period 2016/2017, to calculate absorption equivalent mass concentrations rBC_{PAAS} from the measured absorption coefficients of these samples. The comparison of the deduced light absorbing rBC_{PAAS} mass concentrations with the rBC_{SP2} mass concentrations revealed a wavelength-dependent linear correlation with correlation factors of 1.65, 2.28 and 2.38 for λ=405, 532 and 658 nm, respectively, i.e. significantly different from one. This clearly suggests that other, non-rBC light absorbing aerosol matter is co-deposited in the snow samples.

Additional analyses of an exemplary snow sample using Environmental Scanning Electron Microscopy (ESEM) combined with EDX microanalysis as well as measurements with the Waveband Integrated Bioaerosol Sensor

(WIBS-4) revealed that the larger particles of the snow sample are predominantly of biological origin with lower contributions from mineral dust. These findings point to a possible explanation of the observed difference between the rBC_{SP2} and rBC_{PAAS} mass concentrations and, therefore, to the nature of the co-deposited light absorbing particles in the snow. However, further studies are required including samples from other locations more relevant for climate radiative forcing, to clarify whether biogenic and biological particles are in general main contributors to the visible light absorption in snow and ice surfaces.

7. Acknowledgements

We thank Ludwig Ries, German Environment Agency (UBA) and Gerhard Müller, German Meteorological Service (DWD), Global Observatory Zugspitze/Hohenpeissenberg for providing weather, atmospheric BC and ceilometer data. This work was funded within the Helmholtz Research Program Atmosphere and Climate.

8. Figures

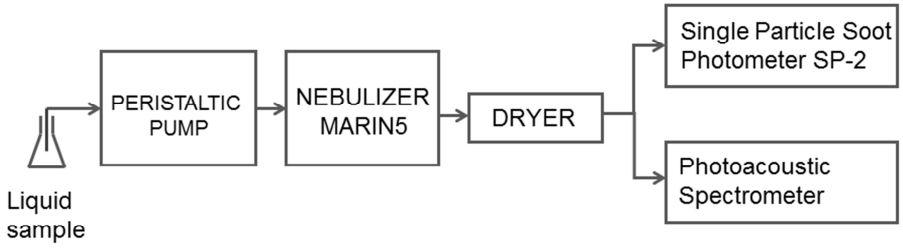

Figure 1: Instrumental setup used in this study.

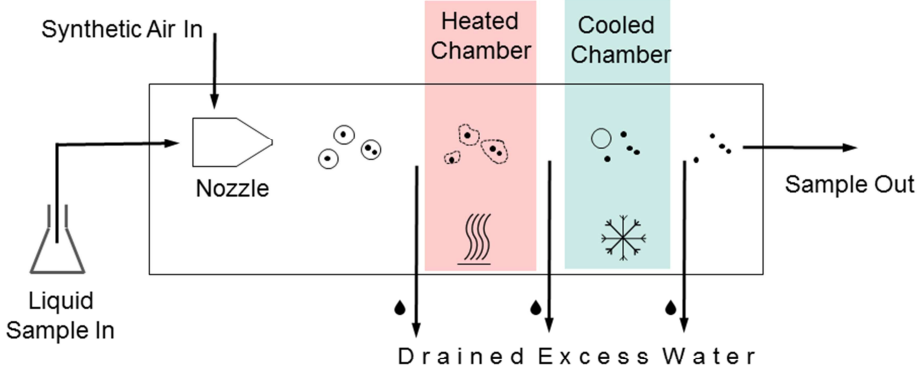

Atmos. Chem. Phys. Discuss., https://doi.org/10.5194/acp-2018-1307
Manuscript under review for journal Atmos. Chem. Phys.
Discussion started: 23 January 2019

Atmospheric Chemistry and Physics Discussions

Figure 2: Principal operation scheme of the CETAC Marin-5 nebulizer.

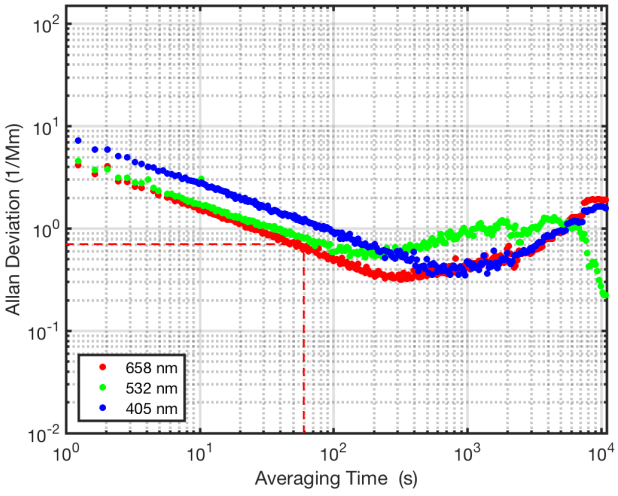

Figure 3: Allan deviation analysis of long-term photoacoustic background measurements. The dashed red lines indicates the typical averaging time applied in the PAAS-3λ measurements and the respective Allan deviation (1σ) of 0.7 1 Mm^{-1}.

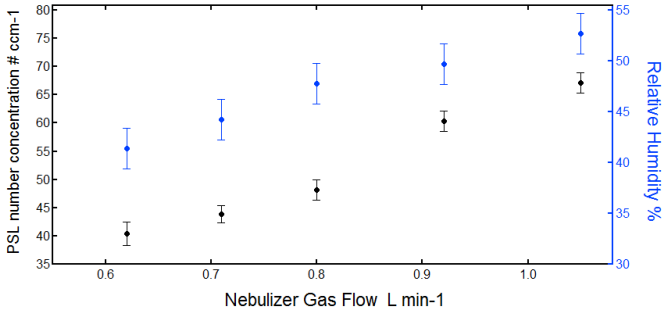

Figure 4: Dependence of the PSL number concentration and relative humidity on the nebulizing gas flow applied in the Marin-5 nebulizer (temperatures of the heated and cooled sections as well as the liquid supply flow were kept constant)

Atmos. Chem. Phys. Discuss., https://doi.org/10.5194/acp-2018-1307
Manuscript under review for journal Atmos. Chem. Phys.
Discussion started: 23 January 2019

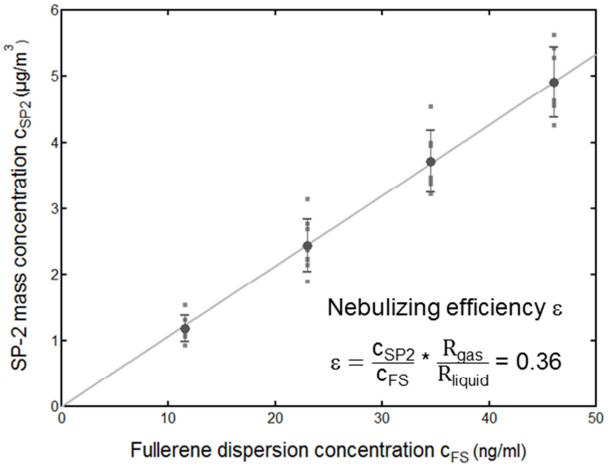

405 **Figure 5: Efficiency ε of the CETAC Marin5 nebulizer for "Fullerene" soot suspensions with defined mass concentrations c_{FS}. The rBC_{SP2} mass concentration was measured in the dry exit gas flow of the nebulizer using a Single Particle Soot Photometer (SP2). See text for details on the preparation of the "Fullerene" soot suspensions.**

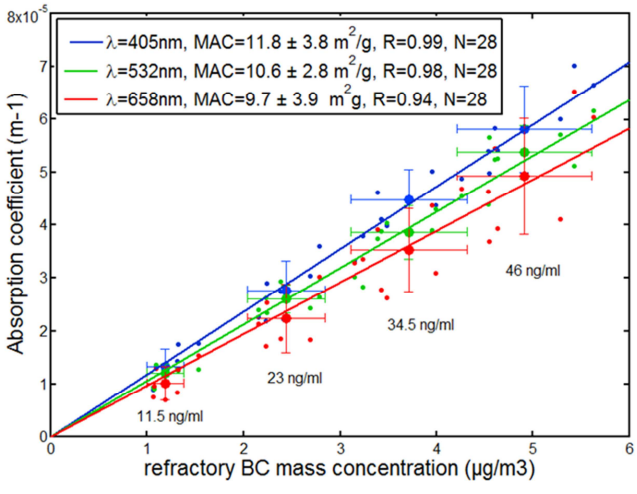

410

Figure 6: Determination of mass specific absorption cross sections (MAC) of re-aerosolized "Fullerene" soot suspensions at 405, 532 and 658 nm. The MAC values are given in the legend and were derived from concurrent measurements of the absorption coefficients using the photo acoustic aerosol absorption spectrometer (PAAS-3λ) and the rBC mass concentrations (SP2)

415

Atmos. Chem. Phys. Discuss., https://doi.org/10.5194/acp-2018-1307
Manuscript under review for journal Atmos. Chem. Phys.
Discussion started: 23 January 2019

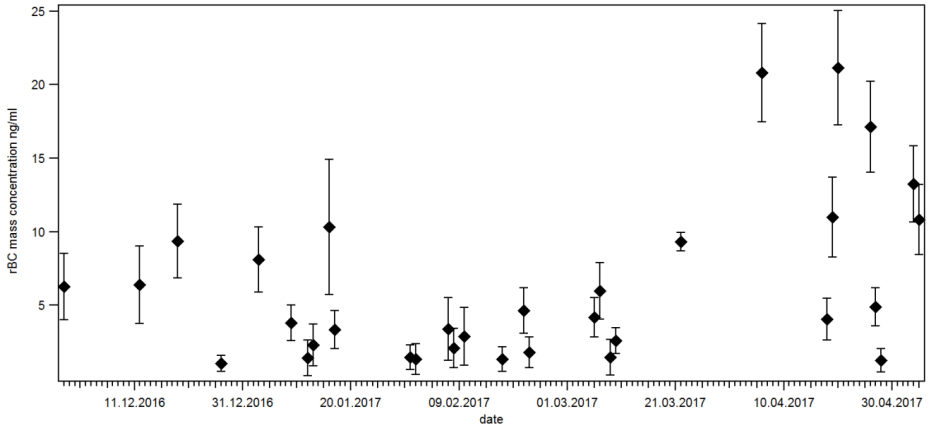

Figure 7: **Refractory black carbon (rBC_{SP2}) mass concentrations determined for snow samples collected at the Environmental Research Station Schneefernerhaus (UFS) during the winter period 2016/2017. The mass concentrations were determined using a Single Particle Soot Photometer (SP2). See text for details concerning sampling and measurement methods.**

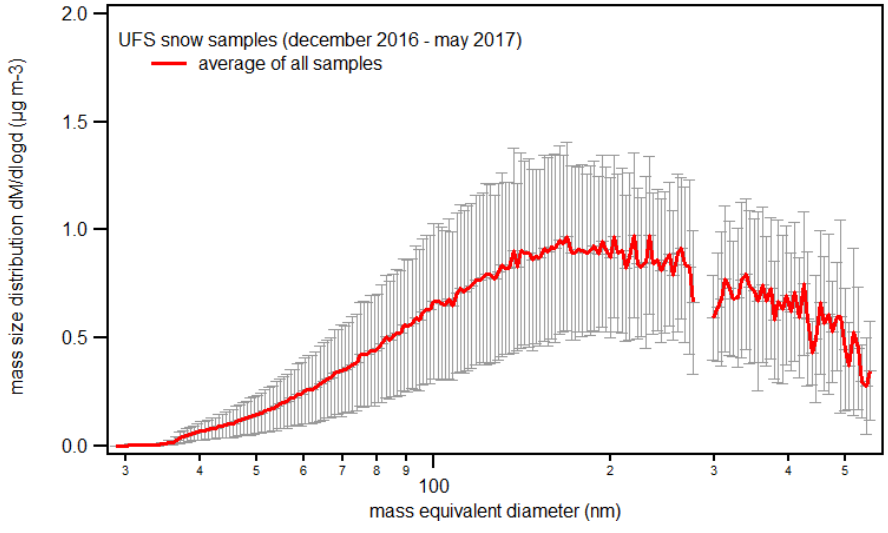

Figure 8:Aerosol mass size distribution averaged over all snow samples.

Atmos. Chem. Phys. Discuss., https://doi.org/10.5194/acp-2018-1307
Manuscript under review for journal Atmos. Chem. Phys.
Discussion started: 23 January 2019

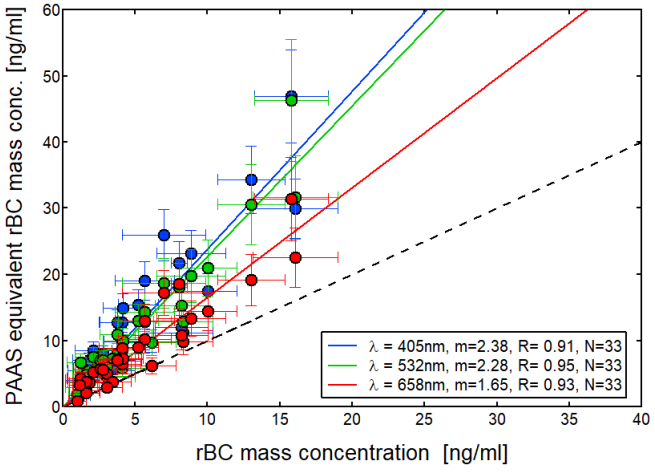

Figure 9: Optically derived rBC $_{PAAS}$ mass concentrations from PAAS-3λ absorption measurements compared to rBC$_{SP2}$ mass concentrations simultaneously measured with the SP2. The 1:1 dashed line indicates the result under the assumption that all particles contributing to visible light absorption are rBC particles with spectral absorption properties equivalent to "Fullerene" soot.

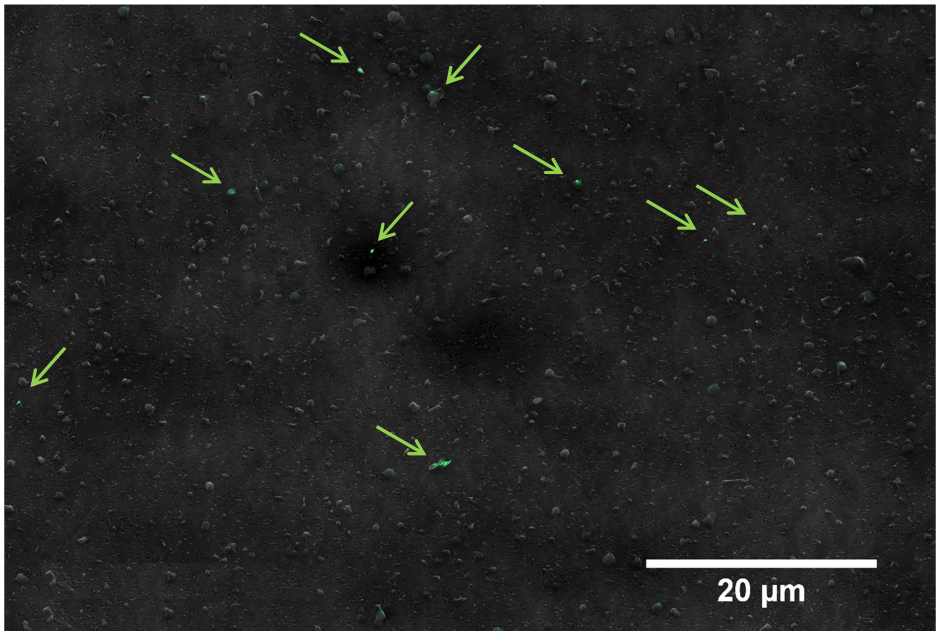

Atmos. Chem. Phys. Discuss., https://doi.org/10.5194/acp-2018-1307
Manuscript under review for journal Atmos. Chem. Phys.
Discussion started: 23 January 2019

Atmospheric Chemistry and Physics Discussions

435 **Figure 10: Overview of residual particles extracted from a snow sample via Marin-5. The image is a false colour overlay from secondary electron (SE) detector (black and white image) and backscatter electron detector, BSED (the green spots). The particles containing elements with higher atomic number are visible as green spots and are highlighted by green arrows.**

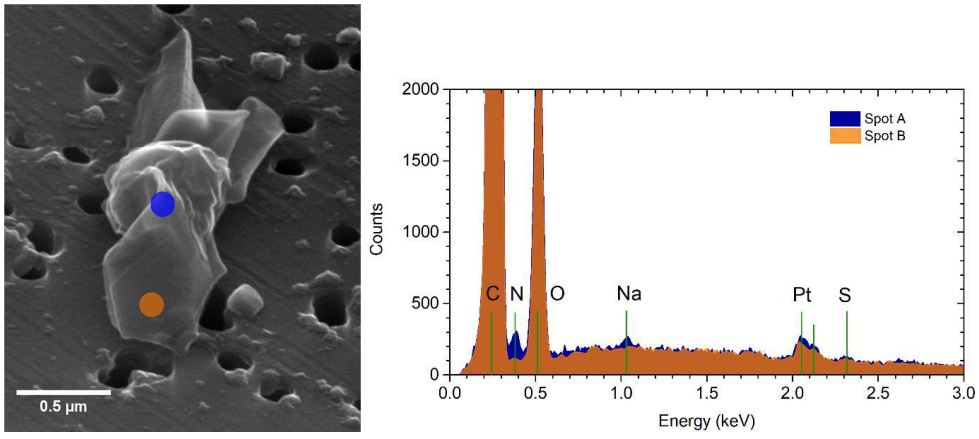

440 **Figure 11: Morphology and composition of biological residual particle extracted from snow sample behind Marin-5 on Nuclepore® filter. Left panel: the SEM secondary electron (SE) image. Right panel: EDX-spectrum obtained from different areas of the particle (marked as colour spots in the image). A clear biogenic signature (N, S, Na) is visible for the central bulky part suggesting intracellular composition (spot A, orange colour), whereas exterior part shows pure carbonaceous compounds (C,O) (spot B, blue colour). Sample coating is responsible for the platinum peak.**

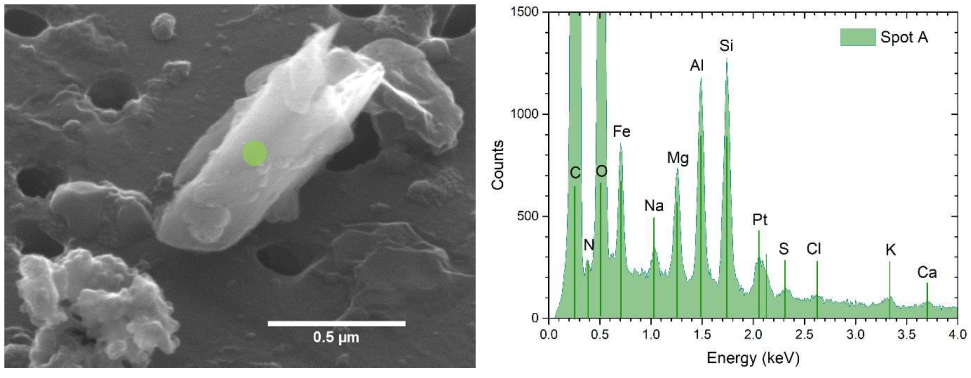

445 **Figure 12 Mineral dust particle extracted from snow sample behind Marin-5 on Nuclepore® filter. Left panel: ESEM image (SE). Right panel: The EDX-spectrum of the particle showing chemical elements characteristic for both mineral dust (Al, Si, Mg, Fe, K, Ca) and for biogenic material (N, Na, Cl, S).**

Atmos. Chem. Phys. Discuss., https://doi.org/10.5194/acp-2018-1307
Manuscript under review for journal Atmos. Chem. Phys.
Discussion started: 23 January 2019

Atmospheric Chemistry and Physics Discussions

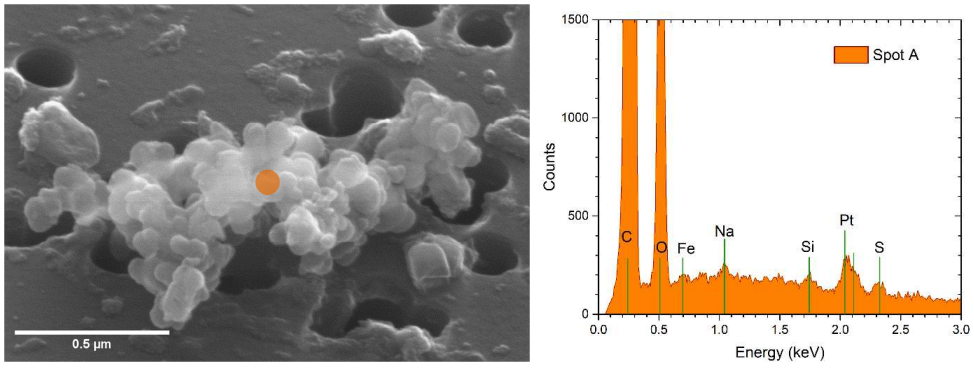

Figure 13. Soot (BC) particle extracted from snow sample behind Marin-5 on Nuclepore® filter. Left panel: ESEM image (SE). Right panel: The EDX-spectrum of the particle, revealing trace elements of Fe, Na, Si, and S.

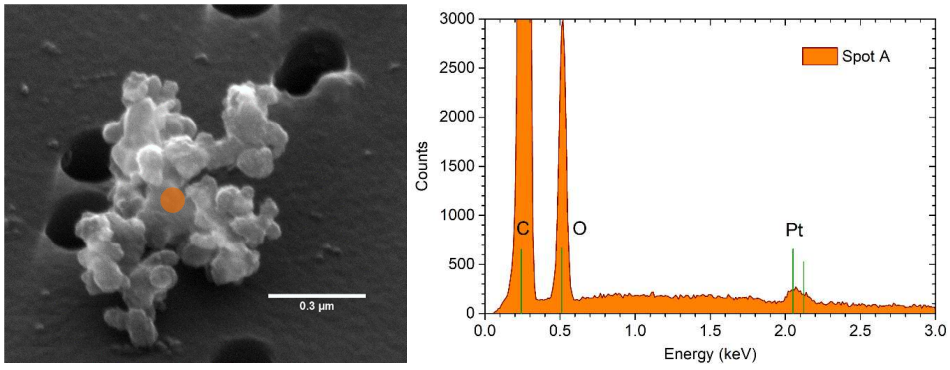

Figure 14. Fullerene particle from aqueous suspension used as standard behind Marin-5 on Nuclepore® filter. Left panel: ESEM image (SE). Right panel: The EDX-spectrum of the particle collected from the spot A, showing pure carbonaceous composition (C,O). Sample coating is responsible for the Pt peak at 2.08 keV.

9. References

Baumgardner, D., Popovicheva, O., Allan, J., Bernardoni, V., Cao, J., Cavalli, F., Cozic, J., Diapouli, E., Eleftheriadis, K., Genberg, P.J., Gonzalez, C., Gysel, M., John, A., Kirchstetter, T.W., Kuhlbusch, T.A.J., Laborde, M., Lack, D., Müller, T., Niessner, R., Petzold, A., Piazzalunga, A., Putaud, J.P., Schwarz, J., Sheridan, P., Subramanian, R., Swietlicki, E., Valli, G., Vecchi, R., Viana, M. (2012) Soot reference materials for instrument calibration and intercomparisons: a workshop summary with recommendations. Atmos. Meas. Tech. 5, 1869-1887.

Bisiaux, M.M., Edwards, R., McConnell, J.R., Curran, M.A.J., Van Ommen, T.D., Smith, A.M., Neumann, T.A., Pasteris, D.R., Penner, J.E., Taylor, K. (2012) Changes in black carbon deposition to Antarctica from two high-resolution ice core records, 1850–2000 AD. Atmos. Chem. Phys. 12, 4107-4115.

Bolch, T., Kulkarni, A., Kääb, A., Huggel, C., Paul, F., Cogley, J.G., Frey, H., Kargel, J.S., Fujita, K., Scheel, M., Bajracharya, S., Stoffel, M. (2012) The State and Fate of Himalayan Glaciers. Science 336, 310.

Bond, T.C., Doherty, S.J., Fahey, D.W., Forster, P.M., Berntsen, T., DeAngelo, B.J., Flanner, M.G., Ghan, S., Kärcher, B., Koch, D., Kinne, S., Kondo, Y., Quinn, P.K., Sarofim, M.C., Schultz, M.G., Schulz, M., Venkataraman, C., Zhang, H., Zhang, S., Bellouin, N., Guttikunda, S.K., Hopke, P.K., Jacobson, M.Z., Kaiser, J.W., Klimont, Z., Lohmann, U., Schwarz, J.P., Shindell, D., Storelvmo, T., Warren, S.G., Zender, C.S. (2013) Bounding the role of black carbon in the climate system: A scientific assessment. Journal of Geophysical Research: Atmospheres 118, 5380-5552.

Chakrabarty, R.K., Moosmüller, H., Chen, L.W.A., Lewis, K., Arnott, W.P., Mazzoleni, C., Dubey, M.K., Wold, C.E., Hao, W.M., Kreidenweis, S.M. (2010) Brown carbon in tar balls from smoldering biomass combustion. Atmos. Chem. Phys. 10, 6363-6370.

Clarke, A.D., Noone, K.J. (1985) Soot in the Arctic snowpack: a cause for perturbations in radiative transfer. Atmospheric Environment (1967) 19, 2045-2053.

Doherty, S.J., Warren, S.G., Grenfell, T.C., Clarke, A.D., Brandt, R.E. (2010) Light-absorbing impurities in Arctic snow. Atmos. Chem. Phys. 10, 11647-11680.

Dumont, M., Brun, E., Picard, G., Michou, M., Libois, Q., Petit, J.R., Geyer, M., Morin, S., Josse, B. (2014) Contribution of light-absorbing impurities in snow to Greenland's darkening since 2009. Nature Geoscience 7, 509.

Fischer, D.A., Smith, G.D. (2018) A portable, four-wavelength, single-cell photoacoustic spectrometer for ambient aerosol absorption. Aerosol Science and Technology 52, 393-406.

Flanner, M.G., Zender, C.S., Hess, P.G., Mahowald, N.M., Painter, T.H., Ramanathan, V., Rasch, P.J. (2009) Springtime warming and reduced snow cover from carbonaceous particles. Atmos. Chem. Phys. 9, 2481-2497.

Flanner, M.G., Zender, C.S., Randerson, J.T., Rasch, P.J. (2007) Present-day climate forcing and response from black carbon in snow. Journal of Geophysical Research: Atmospheres 112.

Flentje, H., Briel, B., Beck, C., Collaud Coen, M., Fricke, M., Cyrys, J., Gu, J., Pitz, M., Thomas, W. (2015) Identification and monitoring of Saharan dust: An inventory representative for south Germany since 1997. Atmospheric Environment 109, 87-96.

Forsström, S., Ström, J., Pedersen, C.A., Isaksson, E., Gerland, S. (2009) Elemental carbon distribution in Svalbard snow. Journal of Geophysical Research: Atmospheres 114.

Garcia-Fernandez, C., Picaud, S., Devel, M. (2015) Calculations of the Mass Absorption Cross Sections for carbonaceous nanoparticles modeling soot. Journal of Quantitative Spectroscopy and Radiative Transfer. 164, 69-81.

Grenfell, T.C., Doherty, S.J., Clarke, A.D., Warren, S.G. (2011) Light absorption from particulate impurities in snow and ice determined by spectrophotometric analysis of filters. APPLIED OPTICS 50.

Hoffer, A., Gelencsér, A., Guyon, P., Kiss, G., Schmid, O., Frank, G.P., Artaxo, P., Andreae, M.O. (2006) Optical properties of humic-like substances (HULIS) in biomass-burning aerosols. Atmos. Chem. Phys. 6, 3563-3570.

Israelevich, P., Ganor, E., Alpert, P., Kishcha, P., Stupp, A. (2012) Predominant transport paths of Saharan dust over the Mediterranean Sea to Europe. Journal of Geophysical Research: Atmospheres 117.

Jacobi, H.W., Lim, S., Ménégoz, M., Ginot, P., Laj, P., Bonasoni, P., Stocchi, P., Marinoni, A., Arnaud, Y. (2015) Black carbon in snow in the upper Himalayan Khumbu Valley, Nepal: observations and modeling of the impact on snow albedo, melting, and radiative forcing. The Cryosphere 9, 1685-1699.

Kaspari, S., Painter, T.H., Gysel, M., Skiles, S.M., Schwikowski, M. (2014) Seasonal and elevational variations of black carbon and dust in snow and ice in the Solu-Khumbu, Nepal and estimated radiative forcings. Atmos. Chem. Phys. 14, 8089-8103.

Katich, J.M., Perring, A.E., Schwarz, J.P. (2017) Optimized detection of particulates from liquid samples in the aerosol phase: Focus on black carbon. Aerosol Science and Technology 51, 543-553.

Kirchstetter, T.W., Thatcher, T.L. (2012) Contribution of organic carbon to wood smoke particulate matter absorption of solar radiation. Atmos. Chem. Phys. 12, 6067-6072.

Li, Y., Chen, J., Kang, S., Li, C., Qu, B., Tripathee, L., Yan, F., Zhang, Y., Guo, J., Gul, C., Qin, X. (2016) Impacts of black carbon and mineral dust on radiative forcing and glacier melting during summer in the Qilian Mountains, northeastern Tibetan Plateau. The Cryosphere Discuss. 2016, 1-14.

Lim, S., Faïn, X., Zanatta, M., Cozic, J., Jaffrezo, J.L., Ginot, P., Laj, P. (2014) Refractory black carbon mass concentrations in snow and ice: method evaluation and inter-comparison with elemental carbon measurement. Atmos. Meas. Tech. 7, 3307-3324.

Linke, C., Ibrahim, I., Schleicher, N., Hitzenberger, R., Andreae, M.O., Leisner, T., Schnaiter, M. (2016) A novel single-cavity three-wavelength photoacoustic spectrometer for atmospheric aerosol research. Atmos. Meas. Tech. 9, 5331-5346.

Linke, C., Möhler, O., Veres, A., Mohácsi, Á., Bozóki, Z., Szabó, G., Schnaiter, M. (2006) Optical properties and mineralogical composition of different Saharan mineral dust samples: a laboratory study. Atmos. Chem. Phys. 6, 3315-3323.

Meinander, O., Kazadzis, S., Arola, A., Riihelä, A., Räisänen, P., Kivi, R., Kontu, A., Kouznetsov, R., Sofiev, M., Svensson, J., Suokanerva, H., Aaltonen, V., Manninen, T., Roujean, J.L., Hautecoeur, O. (2013) Spectral albedo of seasonal snow during intensive melt period at Sodankylä, beyond the Arctic Circle. Atmos. Chem. Phys. 13, 3793-3810.

Moschos, V., Kumar, N.K., Daellenbach, K.R., Baltensperger, U., Prévôt, A.S.H., El Haddad, I. (2018) Source Apportionment of Brown Carbon Absorption by Coupling Ultraviolet–Visible Spectroscopy with Aerosol Mass Spectrometry. Environmental Science & Technology Letters 5, 302-308.

Müller , T., Schladitz, A., Kandler, K., Wiedensohler, A. (2011) Spectral particle absorption coefficients, single scattering albedos and imaginary parts of refractive indices from ground based in situ measurements at Cape Verde Island during SAMUM-2. Tellus B 63, 573-588.

Painter, T.H., Barrett, A.P., Landry, C.C., Neff, J.C., Cassidy, M.P., Lawrence, C.R., McBride, K.E., Farmer, G.L. (2007) Impact of disturbed desert soils on duration of mountain snow cover. Geophysical Research Letters 34.

Phillips, S.M., Bellcross, A.D., Smith, G.D. (2017) Light Absorption by Brown Carbon in the Southeastern United States is pH-dependent. Environmental Science & Technology 51, 6782-6790.

Ramanathan, V., Carmichael, G. (2008) Global and regional climate changes due to black carbon. Nature Geoscience 1, 221.

Risius, S., Xu, H., Di Lorenzo, F., Xi, H., Siebert, H., Shaw, R.A., Bodenschatz, E. (2015) Schneefernerhaus as a mountain research station for clouds and turbulence. Atmos. Meas. Tech. 8, 3209-3218.

Saleh, R., Hennigan, C.J., McMeeking, G.R., Chuang, W.K., Robinson, E.S., Coe, H., Donahue, N.M., Robinson, A.L. (2013) Absorptivity of brown carbon in fresh and photo-chemically aged biomass-burning emissions. Atmos. Chem. Phys. 13, 7683-7693.

Schmitt, C.G., All, J.D., Schwarz, J.P., Arnott, W.P., Cole, R.J., Lapham, E., Celestian, A. (2015) Measurements of light-absorbing particles on the glaciers in the Cordillera Blanca, Peru. The Cryosphere 9, 331-340.

Schwarz, J.P., Doherty, S.J., Li, F., Ruggiero, S.T., Tanner, C.E., Perring, A.E., Gao, R.S., Fahey, D.W. (2012) Assessing Single Particle Soot Photometer and Integrating Sphere/Integrating Sandwich Spectrophotometer measurement techniques for quantifying black carbon concentration in snow. Atmos. Meas. Tech. 5, 2581-2592.

Schwarz, J.P., Gao, R.S., Perring, A.E., Spackman, J.R., Fahey, D.W. (2013) Black carbon aerosol size in snow. Scientific Reports 3, 1356.

Wang, X., Doherty, S.J., Huang, J. (2013) Black carbon and other light-absorbing impurities in snow across Northern China. Journal of Geophysical Research: Atmospheres 118, 1471-1492.

Warren, S.G. (1982) Optical properties of snow. Reviews of Geophysics 20, 67-89.

Warren, S.G. (2013) Can black carbon in snow be detected by remote sensing? Journal of Geophysical Research: Atmospheres 118, 779-786.

Wu, G.-M., Cong, Z.-Y., Kang, S.-C., Kawamura, K., Fu, P.-Q., Zhang, Y.-L., Wan, X., Gao, S.-P., Liu, B. (2016) Brown carbon in the cryosphere: Current knowledge and perspective. Advances in Climate Change Research 7, 82-89.

Zhang, Y., Kang, S., Sprenger, M., Cong, Z., Gao, T., Li, C., Tao, S., Li, X., Zhong, X., Xu, M., Meng, W., Neupane, B., Qin, X., Sillanpää, M. (2018) Black carbon and mineral dust in snow cover on the Tibetan Plateau. The Cryosphere 12, 413-431.

Zhou, Y., Wang, X., Wu, X., Cong, Z., Wu, G., Ji, M. (2017) Quantifying Light Absorption of Iron Oxides and Carbonaceous Aerosol in Seasonal Snow across Northern China. Atmosphere 8 (4), 63.